Phosphoinositide substrates of myotubularin affect voltage-activated Ca(2)(+) release in skeletal muscle

Estela González Rodríguez, Romain Lefebvre, Dóra Bodnár, Claude Legrand, Peter Szentesi, János Vincze, Karine Poulard, Justine Bertrand-Michel, Laszlo Csernoch, Anna Buj-Bello, et al.

Phosphoinositide substrates of myotubularin affect voltage-activated Ca^{2+} release in skeletal muscle

Estela González Rodríguez, **Romain Lefebvre**, **Dóra Bodnár**, **Claude Legrand**, **Peter Szentesi**, **János Vincze**, **Karine Poulard**, **Justine Bertrand-Michel**, **Laszlo Csernoch**, **Anna Buj-Bello**, **Vincent Jacquemond**

Abstract Skeletal muscle excitation–contraction (E–C) coupling is altered in several models of phosphatidylinositol phosphate (PtdIns*P*) phosphatase deficiency and ryanodine receptor activity measured in vitro was reported to be affected by certain PtdIns*P*s, thus prompting investigation of the physiological role of PtdIns*P*s in E–C coupling. We measured intracellular Ca^{2+} transients in voltage-clamped mouse muscle fibres microinjected with a solution containing a PtdIns*P* substrate (PtdIns(3,5)P_2 or PtdIns(3)*P*) or product (PtdIns(5)*P* or PtdIns) of the myotubularin phosphatase MTM1. No significant change was observed in the presence of either PtdIns(5)*P* or PtdIns but peak SR Ca^{2+} release was depressed by ~30% and 50% in fibres injected with PtdIns(3,5)P_2 and PtdIns(3)*P*, respectively, with no concurrent alteration in the membrane current signals associated with the DHPR function as well as in the voltage dependence of Ca^{2+} release inactivation. In permeabilized muscle fibres, the frequency of spontaneous Ca^{2+} release events was depressed in the presence of the three tested phosphorylated forms of PtdIns*P* with PtdIns(3,5)P_2 being the most effective, leading to an almost complete disappearance of Ca^{2+} release events. Results support the possibility that pathological accumulation of MTM1 substrates may acutely depress ryanodine receptor-mediated Ca^{2+} release. Overexpression of a mCherry-tagged form of MTM1 in muscle fibres revealed a striated pattern consistent with the triadic area. Ca^{2+} release remained although unaffected by MTM1 overexpression and was also unaffected by the PtdIns-3-kinase inhibitor LY2940002, suggesting that the 3-phosphorylated PtdIns lipids active on voltage-activated Ca^{2+} release are inherently maintained at a low level, inefficient on Ca^{2+} release in normal conditions.

Keywords Calcium homeostasis · Excitation–contraction coupling · Ryanodine receptor · Sarcoplasmic reticulum Ca^{2+} release · Phosphatidylinositol phosphate

E. González Rodríguez
Departamento de Fisiología, Genética y Microbiología, Universidad de Alicante, Alicante, Spain

R. Lefebvre · C. Legrand · V. Jacquemond (✉)
Centre de Génétique et de Physiologie Moléculaire et Cellulaire, Université Lyon 1, UMR CNRS 5534, Bât. Raphaël Dubois, 43 boulevard du 11 novembre 1918, F69622, Villeurbanne, France
e-mail: vincent.jacquemond@univ-lyon1.fr

D. Bodnár · P. Szentesi · J. Vincze · L. Csernoch
Department of Physiology, University of Debrecen, Debrecen, Hungary

K. Poulard · A. Buj-Bello
Department of Research and Development, Généthon, INSERM, Evry, France

J. Bertrand-Michel
Lipidomic Core Facility, Metatoul Platform, INSERM U1048, Université de Toulouse, Université Paul Sabatier, Toulouse, France

Introduction

The function of phosphoinositides had for a long time remained limited to the possible role of phosphatidylinositol 4,5-bisphosphate (PtdIns(4,5)P_2) as a substrate of phospholipase C to produce inositol-trisphosphate (Ins(1,4,5)P_3) and diacylglycerol. The last decade has seen a remarkable expansion of the concept so as to now include the role of PtdIns*P*s phosphorylated in the 3-OH position, which control a wide array of cellular functions including membrane trafficking, cytoskeleton remodeling, protein docking, and membrane transport (for review, see [12]), and numerous studies have also

revealed the fundamental role of PtdIns*P*s in regulating ion channel activity (for reviews, see [25, 35]).

Skeletal muscle cells contract in response to depolarizing changes of their plasma membrane voltage: action potentials fired at the end-plate of the muscle fibres propagate throughout the transversal (t-) tubule system: coupling between membrane depolarization and contraction occurs within the triad regions where one t-tubule faces two terminal cisternae of sarcoplasmic reticulum (SR). There, depolarization changes the conformation of the dihydropyridine receptor (DHPR, the Cav1.1 protein, the voltage-sensing component of the system) which opens up the SR calcium release channel (type 1 ryanodine receptor, RyR1) through protein–protein conformational coupling. Upon membrane repolarization, RyR1 channels close, and muscle relaxation occurs due to cytosolic Ca^{2+} extrusion driven by the SR Ca^{2+} pump.

This basic functional scheme is either known or presumed to be controlled, regulated or modulated by a wide array of accessory proteins and messenger molecules (for review, see [22]). The possible role of PtdIns*P*s in the regulation of Ca^{2+} homeostasis and excitation–contraction (E–C) coupling in muscle remained elusive until recent years. Indeed, if one excludes the controversies related to the possible role of the Ins(1,4,5)P_3 pathway (e.g., [16]), only very few studies in the 1990s suggested that PtdIns(4,5)P_2 could affect the SR Ca^{2+} release process [6, 20, 29]. However, recent data from transgenic models of PtdIns*P*-phosphatase deficiency, specifically MTM1 (myotubularin) and parent proteins ("myotubularin and myopathy related" phosphatases [MTMRs]; see [3]) provided completely unanticipated insights into the field: in humans, more than 200 mutations of the gene encoding MTM1 are associated with X-linked myotubular myopathy (see [23]), characterized by very severe muscle weakness and consequent fatal outcome, often within weeks following birth [30]. The link between MTM1 deficiency and muscle weakness remained obscure until muscle fibres from MTM1-deficient mice were shown to suffer from a critically defective E–C coupling process [1]. Concurring data from a MTM1-deficient zebrafish model were provided by Dowling et al. [14]. In mouse, MTM1-deficient muscle fibres yield defects in the internal membrane system structure and organization, reduced levels of DHPR and RyR1 and a strong decrease in the amplitude of voltage-activated cytosolic Ca^{2+} signals. This functional alteration is certainly the direct cause of muscle weakness in the affected patients. Results by Al-Qusairi et al. [1] also demonstrated that SR Ca^{2+} content and cytosolic Ca^{2+} removal capabilities are unaltered in MTM1-deficient muscle fibres. At the functional level, the disease status thus appears to specifically affect the SR Ca^{2+} release process.

The internal membrane architecture defects may contribute to this alteration but are likely not the sole explanations: inner structure alterations are common features of several types of muscle disorders and are already observed in young MTM1-deficient mice which have limited defects in muscle function [1]. Furthermore, MTMR14 deficiency in zebrafish is also associated with defective E–C coupling, but without the inner-membrane-systems architecture defects observed in absence of MTM1 [13]. The reduction in the level of RyR1 would also, intuitively, be expected to play a role in muscle weakness, but actually the question of how much of the normal RyR1 content is necessary to sustain E–C coupling in muscle is far from clearly established. It is important to point out in this respect that several human muscle diseases due to *RYR1* mutations have been shown to be associated with a more severe reduction in RyR1 than observed under the conditions of MTM1 deficiency; the fact that severe RyR1 reduction in these cases was associated with a much lesser impact on muscle function and life expectancy [27, 37–39] seems to indicate that this may not be the critical issue determining the severity of myotubular myopathy.

One obvious possibility is that the E–C coupling defect results from altered PtdIns*P*s metabolism due to the loss of MTM1 PtdIns*P*-phosphatase activity. It is supported by results from Shen et al. [34] showing that loss of another PtdIns*P*-phosphatase (MTMR14) is responsible for alterations of intracellular Ca^{2+} homeostasis in muscle, attributable to defective regulation of RyR1 channel activity by PtdIns*P*s. Recent data also indicate that muscle weakness associated with aging may be due to altered Ca^{2+} homeostasis because of a reduced level of MTMR14 [33]. This trend of data thus tends to suggest a role for PtdIns*P*s in the regulation of skeletal muscle Ca^{2+} homeostasis and E–C coupling under normal conditions and a role for alteration of this regulation in certain muscle diseases. We looked here for a direct evidence that PtdIns*P*s are physiologically involved in the regulation of Ca^{2+} and E–C coupling in normal muscle. We demonstrate that MTM1 main PtdIns*P* substrates inhibit the function of E–C coupling while maneuvers intended to reduce the level of these 3-OH phosphorylated PtdIns have no effect.

Materials and methods

All experiments and procedures were in accordance with the guidelines of the local animal ethics committee of University Lyon 1 and University of Debrecen, of the French Ministry of Agriculture (87/848) and of the European Community (86/609/EEC).

In vivo transfection

An expression plasmid encoding wild-type mouse MTM1 fused N-terminally to mCherry was constructed using the pmCherry-C1 vector (Clontech, Mountain View, CA, USA). Swiss OF1 male mice that were 1–2 months old were used. Transfection was performed in the *flexor digitorum brevis*

(*fdb*) and interosseus muscles of the animals. Details of the procedure used for in vivo electroporation are given in Electronic supplementary material. Experimental observations and measurements were carried out 7–10 days later.

Preparation of isolated muscle fibres

Single fibres were isolated from the *fdb* and interosseus muscles from mouse using a previously described procedure [18]. In brief, mice were killed by cervical dislocation before removal of the muscles. Muscles were treated with collagenase (Sigma, type 1) for 60 min at 37°C. Single fibres were then obtained by triturating the muscles within the experimental chamber. They were dispersed on the glass bottom of a 50-mm-wide culture μ-dish (Biovalley, Marne la Vallée, France). For intracellular Ca^{2+} measurements under voltage-clamp conditions, fibres were first partially insulated with silicone grease as described previously [18]; in brief, fibres were embedded within silicone so that only a portion of the fibre extremity was left out of the silicone. Under these conditions, fibres remained well maintained on the bottom of the chamber and this allowed whole-cell voltage clamp to be achieved on the silicone-free extremity of the fibre. Once partially embedded within silicone, indo-1 or fluo-4 was introduced into the myoplasm through local pressure micro-injection with a micropipette containing 1 mM of the dye. Indo-1 was dissolved in the standard intracellular-like solution (see Solutions) whereas fluo-4 was dissolved in a solution containing 100 mM EGTA and 40 mM $CaCl_2$. Details regarding the use of EGTA are given in the Electronic supplementary material. Microinjection was always performed within the silicone-embedded part of the fibre, away from the silicone-free end portion under study. Following diffusion and equilibration within the cytoplasm, this was believed to achieve a final cytoplasmic concentration or indo-1 or fluo-4 within the 100 μM range and of EGTA within the 10 mM range, respectively (for details concerning micro-injections, see [10]). Experiments were usually performed on fibres from the *fdb* muscle; only when testing the effect of MTM1 overexpression were a few control and MTM1-positive fibres from interosseus muscles used. For all experimental situations, control fibres (either untreated with the tested reagent or non-expressing the tested transfected gene) were always from the same muscles as the tested fibres. All experiments were performed at room temperature (20–22°C).

Electrophysiology

An RK-400 patch-clamp amplifier (Bio-Logic, Claix, France) was used in whole-cell voltage-clamp configuration. Fibres were bathed in the TEA-containing extracellular solution (see Solutions). Command voltage pulse generation was achieved with an analog–digital converter (Digidata 1440A; Axon Instruments, Foster City, CA, USA) controlled by pClamp 9 software (Axon Instruments). Voltage-clamp was performed with a microelectrode filled with the intracellular-like solution (see Solutions). The tip of the microelectrode was inserted through the silicone, within the insulated part of the fibre. Analog compensation was systematically used to decrease the effective series resistance. Membrane depolarizing steps were applied from a holding command potential of −80 mV, unless otherwise specified. Removal of the linear leak and capacitive components of the current changes elicited by a depolarizing pulse was achieved as previously described [8, 32]. Details of the procedures used for membrane current analysis are given in the Electronic supplementary material.

Fluorescence measurements in voltage-clamped fibres

Indo-1 fluorescence was measured on an inverted Nikon Diaphot epifluorescence microscope equipped with a commercial optical system allowing the simultaneous detection of fluorescence at 405 nm (F405) and 485 nm (F485) by two photomultipliers (IonOptix, Milton, MA, USA), upon 360 nm excitation. Background fluorescence at both emission wavelengths was measured next to each fibre tested and was then subtracted from all measurements.

Confocal fluorescence measurements were done using a Zeiss LSM 5 Exciter confocal microscope equipped with a × 63 oil immersion objective (numerical aperture 1.4). Fluo-4 excitation was provided by the 488 nm line of an argon laser and a 505- to 600-nm band-pass filter was used on the detection channel. For detection of mCherry fluorescence the excitation was from the 543-nm line of a HeNe laser and fluorescence was collected above 560 nm. Intracellular $[Ca^{2+}]$-related fluorescence changes were imaged by using the line-scan mode of the system with the line parallel to the longitudinal fibre axis. The majority of images were taken with a scanning frequency of 1.15 ms per line. Image processing and analysis was performed using Image/J (NIH, USA) and Microcal Origin (Microcal Software Inc., Northampton, MA, USA).

$[Ca^{2+}]$ and Ca^{2+} release calculation in intact fibres

For indo-1 fluorescence signals, the standard ratio method was used with the parameters: $R=F_{405}/F_{485}$, with R_{min}, R_{max}, K_D and β having their usual definitions. Results were either expressed in terms of indo-1% saturation or in actual free Ca^{2+} concentration; in vivo values for R_{min} and β were measured using procedures previously described [18]. R_{max} was determined at the end of the experiments after damaging the fibre under study with a thin needle until complete contracture. An estimation of the Ca^{2+} release flux underlying the calculated global $[Ca^{2+}]$ transients was performed as described previously [9, 31]. Details of the procedure used for Ca^{2+} release calculation are given in the Electronic supplementary material.

Fluo-4 changes in fluorescence were expressed as F/F_0, where F_0 is the resting (or baseline) fluorescence level. Changes in [Ca^{2+}] were calculated from the fluo-4 signals using the pseudo-ratio equation [5] assuming a basal [Ca^{2+}] of 100 nM and a K_d of fluo-4 for Ca^{2+} of 1 μM [17]. No correction was made for the fluo-4 binding kinetics.

Measurements of SR Ca^{2+} content in intact fibres

For this, we used a protocol similar to the one we described in a previous study [1]. In brief, the cytosol of *fdb* fibres was dialyzed through the voltage-clamp pipette with the intracellular-like solution also containing 20 mM EGTA, 8 mM Ca, 0.2 mM indo-1 with or without PtdIns(3)*P* (0.1 mM). Following a 30-min period of equilibration, five 200-ms-long pulses from −80 to +10 mV were applied every minute, while the portion of fibre under study was superfused with the standard extracellular solution using a local perfusion system operating by gravity. The portion of fibre was then superfused for 2 min with the extracellular solution also containing 0.1 mM cyclopiazonic acid (CPA) in order to block SR Ca^{2+} uptake. Pulses of 200 ms duration from −80 to + 10 mV were then applied again, at a frequency of 1 Hz in order to rapidly release SR Ca^{2+}. Under these conditions, following the first pulses in the presence of CPA, indo-1 saturation reached an elevated steady level indicating that most of the SR content had been released. We took the difference between this elevated steady level and the initial resting saturation level in each fibre to estimate how much calcium had been released, assuming that saturation of EGTA was the same as saturation of indo-1 and that 20 mM EGTA was present in the cytosol.

Measurements of elementary Ca^{2+} release events (ECREs) in permeabilized muscle fibres

Isolated mouse skeletal muscle fibres from the *fdb* were permeabilized with saponin and loaded with 0.1 mM fluo-3 using previously described experimental solutions and procedures [11]. Briefly, fibres were bathed in a relaxing solution (see Solutions) containing 0.002% saponin for 2–3 min. Permeabilization of the surface membrane was monitored by imaging the fluorescence of fluo-3 present at a concentration of 0.1 mM in the solution. This solution was then replaced by the recording solution (see Solutions). Images were captured with a Zeiss LSM 510 LIVE confocal microscope (Zeiss, Oberkochen, Germany) equipped with a 40× oil immersion objective (NA=1.3). Fluo-3 was excited with the 488-nm line of an argon laser and the emitted fluorescent light was measured at wavelengths >505 nm. Unless otherwise specified, 15 min following application of the recording solution, eight consecutive series of 200 512×512 (x,y) images captured every 67 ms were collected in each tested fibre. Test experiments were carried out in the presence of 0.1 mM of a given PtdIns*P* species (diC8; Echelon Biosciences Inc.) in the recording solution. For each series of test measurements in fibres bathed in the presence of a given PtdIns*P*, a parallel series of control measurements (with no PtdIns*P*) was made using fibres isolated from the same muscles. For analysis, results from a given PtdIns*P* condition were compared to those from the corresponding group of control fibres. Measurements with PtdIns(3,5)P_2, PtdIns(3)*P*) and PtdIns(5)*P* were performed within the same series of experiments whereas measurements with PtdIns were performed 6 months later.

ECRE detection and analysis were performed using modified methods and algorithms described previously by Szabó et al. [36]: details are given in the Electronic supplementary material.

Quantification of PtdIns*P*s in muscle fibres

The concentration level of endogenous PtdIns*P*s in muscle fibres was achieved using the high-performance liquid chromatography–mass spectrometry technique described by Clark et al. [7]. Experiments were conducted at the Lipidomic Core Facility Platform at University of Toulouse. Measurements were carried out on muscle fibres isolated from five *fdb* muscles. Muscles were treated with collagenase as described above. Each *fdb* muscle was then mechanically triturated in a 2-ml volume of Tyrode solution containing 10 mM EGTA. Mechanical trituration of each muscle was achieved so as to release a large number of muscle fibres in the sample; the total number of muscle fibres isolated from each muscle was determined from counting the fibres present in a 50-μl volume of this solution. Each sample was frozen in liquid nitrogen and maintained at −80°C until use. High-performance liquid chromatography was performed on each sample using an Agilent 1290 Infinity, equipped with an autosampler, coupled online to an Agilent 6460 triple quadrupole MS (Agilent Technologies) equipped with electrospray ionization (ESI) source. ESI was performed in positive ion mode. After optimization, the source parameters used were as follows: source temperature was set at 250°C, nebulizer gas (nitrogen) flow rate was 12 l/min, sheath gas temperature was 250°C, sheath gas (nitrogen) flow rate was 12 l/min and the spray voltage was adjusted to 4,000 V. Results expressed in ng of PtdIns*P* PtdInsP_2 and PtdInsP_3 present in each sample were converted into concentration level *per* muscle fibre using the total number of fibres estimated in each sample and assuming a fibre volume of ~2×10^{-7} ml (from an average fibre diameter and length estimated to be 25 and 300 μm, respectively, assuming fibres to be cylindrical).

Solutions

The extracellular solution used for whole-cell voltage-clamp contained (in mM) 140 TEA-methanesulfonate, 2.5 $CaCl_2$, 2 $MgCl_2$, 10 TEA-HEPES and 0.002 tetrodotoxin. In certain

series of measurements, 4-aminopyridine was also present at 1 mM. The intracellular-like solution for whole-cell voltage-clamp contained (in mM) 120 K-glutamate, 5 Na_2 ATP, 5 Na_2 phosphocreatine, 5.5 $MgCl_2$, 5 glucose, 5 HEPES. For indo-1 fluorescence measurements, the dye was present at 1 mM in the injected intracellular-like solution. PtdIns*P*s (diC8; Echelon Biosciences Inc.) were present at 1 mM in the injected solution. LY294002 (Echelon Biosciences Inc.) was prepared in DMSO at a concentration of 10 mM and diluted at 1 mM in the injection solution; DMSO at the same concentration was injected in the control fibres from that series of measurements. For confocal line-scan fluo-4 fluorescence measurements under voltage-clamp conditions, the injected solution contained (in mM) 100 EGTA, 40 $CaCl_2$ and 1 fluo-4. For measurements of ECREs in permeabilized fibres, the relaxing solution contained (in mM) 125 K-glutamate, 10 HEPES, 1 EGTA, 6 $MgCl_2$, 5 Na_2-ATP, 10 Na-phosphocreatine, 10 glucose, 0.13 $CaCl_2$ and the recording solution contained (in mM) 95 K_2SO_4, 10 HEPES, 1 EGTA, 6 $MgCl_2$, 5 Na_2-ATP, 10 Na-phosphocreatine, 10 glucose, 0.13 $CaCl_2$, respectively. All solutions were adjusted to pH 7.20.

Statistics

Least-squares fits were performed using a Marquardt–Levenberg algorithm routine included in Microcal Origin (Originlab, Northampton, MA, USA). Data values are presented as means ± SEM for n fibres. Statistical significance was determined using a Student's t-test: *$p \leq 0.05$, **$p \leq 0.01$, ***$p \leq 0.001$.

Results

PtdIns(3,5)P_2 and PtdIns(3)P depress voltage-activated Ca^{2+} release

Since MTM1 deficiency produces a severe impairment of E–C coupling [1], we were specifically interested in the effect of substrates and products of its phosphatase activity. Soluble forms of PtdIns(3,5)P_2, PtdIns(3)P, PtdIns(5)P or PtdIns were thus micro-injected in separate batches of single isolated muscle fibres and intracellular Ca^{2+} was measured under voltage-clamp conditions. PtdIns*P*s injection was performed so as to reach a final concentration expected to be within the 100 μM range, matching the maximum levels of PtdIns*P*s shown to affect [^{3}H] ryanodine binding to SR as well as single channel activity of RyR1 in bilayer [34]. Mean resting [Ca^{2+}] did not differ between control fibres (0.16±0.02 μM, n=16) and any of the PtdIns*P*s-injected fibre group, but was significantly elevated in fibres injected with either PtdIns(3,5)P_2 (0.21±0.02 μM, n=8) or PtdIns(3)P (0.20±0.02 μM, n=8) as compared to fibres injected with PtdIns(5)P (0.14±0.01 μM, n=7) or PtdIns (0.12±0.02 μM, n=6).

In order to evaluate the effect of the different PtdIns*P*s on the properties of Ca^{2+} transients and Ca^{2+} release, fibres were stimulated by a voltage-clamp protocol consisting in successive 20-ms-long depolarizing pulses of increasing amplitude from −80 mV. This protocol was repeated five times in each fibre and the traces were averaged. Figure S1 shows an illustrative average indo-1 saturation trace obtained in a control fibre in response to this protocol as well as the corresponding Ca^{2+} release trace calculated as described in Materials and methods and an expanded view of a portion of that same trace centered on the last transient. Figure 1 shows mean indo-1 saturation traces obtained in response to this protocol in the different batches of fibres. The grey shading superimposed to each trace corresponds to the SEM. There was no obvious alteration in the qualitative kinetic properties of the transients in the presence of any of the PtdIns*P*s. However, the peak amplitude was depressed in the presence of PtdIns(3)P and, to a lesser extent also in the presence of PtdIns(3,5)P_2. The graphs on the right side in Fig. 1 report the voltage dependence of the mean value for peak Ca^{2+} release in each corresponding condition. The voltage dependence of peak Ca^{2+} release was fitted in each fibre with a Boltzmann function. Corresponding mean values for maximum peak Ca^{2+} release ($d[Ca]_T/dt$ max), voltage of half-activation ($V_{0.5}$) and steepness factor (k) are reported in Fig. 2; as compared to control fibres, maximum Ca^{2+} release was depressed by 50% and 30% in the presence of PtdIns(3)P (p<0.001) and PtdIns(3,5)P_2 (p=0.02), respectively, whereas the steepness factor was slightly but significantly enhanced in the presence of PtdIns(3,5)P_2 (p=0.001) and PtdIns(5)P (p=0.03). It is worth stressing that indo-1 is a rather high-affinity Ca^{2+} dye with limited kinetic properties precluding fully reliable detection of large fast changes in [Ca^{2+}]. Still, when used in combination with voltage-clamp, the possibility of measuring Ca^{2+} transients in response to small levels of depolarization for which the dye remains far from saturation limits the high-saturation hazardous effects. In other words indo-1 limitations should in no case affect the qualitative effects of PtdIns*P*s observed here but the exact extent of inhibition of Ca^{2+} release by PtdIns(3)P and PtdIns(3,5)P_2 may have been somewhat underestimated.

Analysis of the decay phase of the transients (see Fig. S2) indicated that the rate of cytosolic Ca^{2+} removal tended to be significantly slower in fibres injected with PtdIns(3)P; since Ca^{2+} release was calculated assuming identical Ca^{2+} removal properties in all fibre groups, this likely indicates that the extent of decrease in peak Ca^{2+} release in PtdIns(3)P injected fibres was underestimated.

One important issue was whether the depressed Ca^{2+} release resulted from a depleted SR Ca^{2+} content. In order to address the question a specific series of experiments was

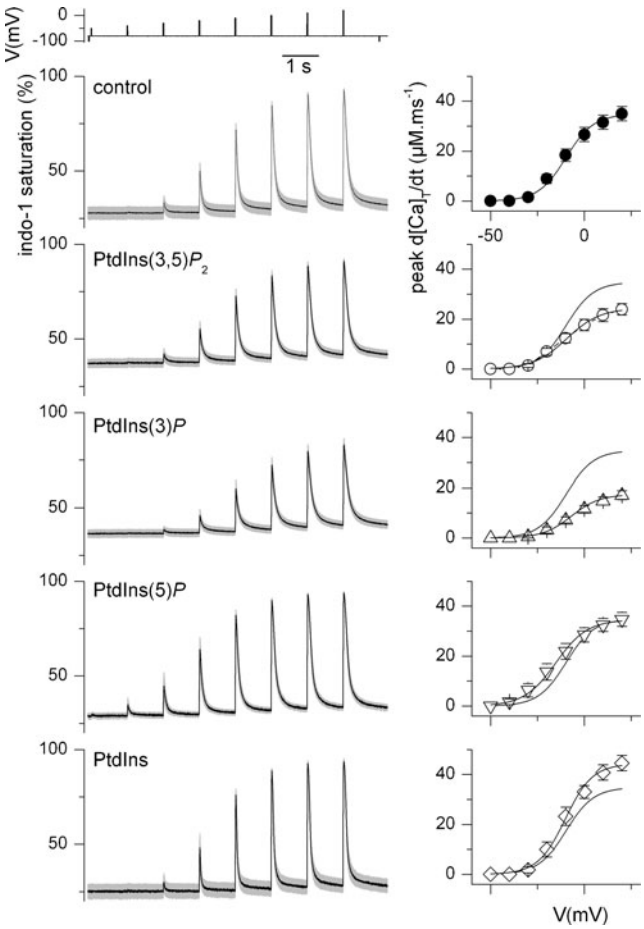

Fig. 1 Voltage-activated Ca^{2+} release in muscle fibres injected with PtdIns*P*s. *Left panel*: mean (±SEM, *grey shading*) indo-1 saturation signal measured in the groups of muscle fibres injected with, from top to bottom, indo-1 with no PtdIns*P* (n=16) and indo-1 with PtdIns(3,5)P_2 (n=8), PtdIns(3)*P* (n=8), PtdIns(5)*P* (n=7), PtdIns (n=6), respectively. The voltage-clamp pulse protocol is shown at the *top*. The voltage-dependence of mean values for peak Ca^{2+} release in each condition is shown on the *right*, next to each corresponding indo-1 trace. The trace superimposed to each set of data points corresponds to a Boltzmann function calculated with the mean parameters obtained from an individual fit of the function to the data points in each fibre

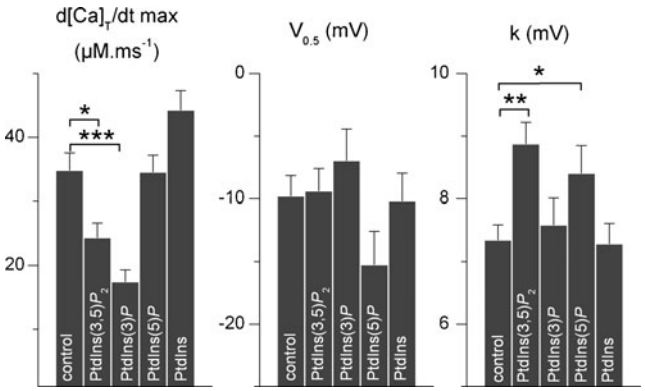

Fig. 2 Mean values for the Boltzmann parameters of the voltage-dependence of Ca^{2+} release in PtdIns*P*s-injected fibres. Mean values for maximal peak rate of Ca^{2+} release, half-activation voltage and steepness were obtained in the different groups of PtdIns*P*s injected fibres from a Boltzmann fit to the peak Ca^{2+} release versus voltage data in each fibre

performed to estimate the SR Ca^{2+} content in control fibres and in fibres containing the PtdIns*P* producing the most effective depression of Ca^{2+} release (PtdIns(3)*P*). For this, we used a protocol consisting in releasing the SR Ca^{2+} content into the cytosol in the presence of a large concentration of EGTA (see Materials and methods). From measurements taken in five control fibres and in six fibres equilibrated with 0.1 mM PtdIns(3)*P* in the intracellular solution, the mean SR Ca^{2+} content was 2.1±0.5 and 2.6±0.4, respectively, which was not statistically different. This thus tends to exclude the possibility that voltage-activated SR Ca^{2+} release was depressed as a consequence of a decreased SR content.

In order to test whether the function of the DHPR was affected and potentially responsible for the above-described effects, we analyzed the membrane current records taken during these experiments. Results from this analysis are presented in Fig. S3 and in the corresponding text section of the Electronic supplementary material. Overall, the results demonstrated that neither the voltage-sensing function of the DHPR nor its Ca^{2+} channel function was substantially affected by PtdIns*P*s.

While testing the effect of PtdIns*P*s on Ca^{2+} transients, we questioned the possibility that voltage-dependent inactivation of Ca^{2+} release would be affected. To test for this, we measured indo-1 transients in response to a pair of 20-ms long pulses to −20 and 0 mV from increasing levels of holding potential. The two pulses were used in order to ensure that heavy saturation of indo-1 for the largest pulse would not hinder detection of a decrease in the Ca^{2+} transient amplitude when changing the holding potential towards more depolarized levels. The pulse protocol and the corresponding mean (±SEM) indo-1 saturation traces obtained in control fibres are shown in Fig. S4a,b. In each fibre, the peak Ca^{2+} transient amplitude calculated from the indo-1 signal was normalized to the initial value measured from the holding potential of −80 mV. We found no indication that any of the four tested PtdIns*P*s affected the inactivation process; this is illustrated in Fig. S4c, where the mean normalized peak amplitude of the Ca^{2+} transient versus the holding potential in the different groups of fibres are shown. Fitting a Boltzmann function to the data in each fibre gave mean values for half-inactivation voltage and steepness factor that did not differ between control fibres and any of the four groups of PtdIns*P*s-injected fibres.

PtdIns(3,5)P_2, PtdIns(3)*P* and PtdIns(5)*P* depress the frequency of ECREs in permeabilized muscle fibres

Measurement of spontaneous ECREs in permeabilized muscle fibres provides a way to study the functional properties of the ryanodine receptor in its native environment, freed from the DHPR control (e.g., [19, 26]). We used this approach to

test whether PtdIns*P*s would directly affect RyR-mediated Ca^{2+} release activity and get insights into the underlying mechanism. Spontaneous ECREs were measured using fast confocal (x,y) imaging, 15 min following equilibration of fibres with a given PtdIns*P* and properties of the events were compared to those of fibres from the same muscles equilibrated for 15 min with the standard experimental solution. Figure 3a shows an illustrative (x,y) confocal record of fluo-3 fluorescence from one fibre in each group. Each frame represents the cumulated ECRE activity recorded during a series of 200 consecutive images, covering a period of approximately 13 s. There was a substantial reduction of the number of detected ECREs in the fibres equilibrated with PtdIns(3,5)P_2, PtdIns(3)*P* and PtdIns(5)*P*, the effect being most important with PtdIns(3,5)P_2. Figure 3b shows the mean values for the measured parameters. ECRE frequency was strongly depressed in the presence of each of the three tested phosphorylated forms of PtdIns*P* with the drop amounting to 98% in the presence of PtdIns(3,5)P_2. The mean ECRE amplitude was slightly but significantly increased in the presence of PtdIns(5)*P* whereas the FWHM along both the x and y directions was depressed by ~10% in the presence of PtdIns(3,5)P_2. Altogether, the tested PtdIns*P*s appeared to modestly, if any, affect the individual ECRE amplitude and spatial properties while severely impairing the occurrence of the events. From that series of measurements we could also check that the observed decrease in ECRE frequency in the presence of PtdIns(3,5)P_2, PtdIns(3)*P* and PtdIns(5)*P* was present right when we started taking measurements: for instance, during the first series of 200 images, the average ECRE frequency was depressed by 92% in fibres equilibrated with PtdIns(3,5)P_2 as compared to the frequency in their control counterparts.

We also performed a specific series of measurements designed to study the time course of ECRE activity earlier in time following application of the PtdIns*P* that was found the most effective on ECRE frequency (PtdIns(3,5)P_2). This was expected to reveal whether or not a putative PtdIns(3,5)P_2-induced early transient increase in spark activity may have occurred during our experiments so as to induce SR Ca^{2+} depletion and thus compromise ECRE occurrence during the measurements that were started 15 min following application of the recording solution. For this, we started taking images 3 min following application of the recording (either control or PtdIns(3,5)P_2-containing) solution and a series of 200 images was then taken every 3 min. ECREs were counted within each series. Results from measurements in five control fibres and three fibres in the presence PtdIns(3,5)P_2 showed that there was no significant change in spark frequency over time in both groups of fibres (not illustrated). In terms of absolute values, the mean frequency in the three PtdIns(3,5)P_2 fibres was depressed by 65–80% as compared to the corresponding values in the control fibres. Although this was somewhat less of an effect than in the set of measurements illustrated in Fig. 3, results clearly demonstrated that there was no sign whatsoever of any stimulating effect of PtdIns(3,5)P_2 on ECRE activity. Finally, in two of the three fibres tested in the presence of PtdIns(3,5)P_2, the experiment was ended by exchanging the test solution with the same solution also containing 0.4 mM 4-chloro-*m*-cresol (CMC) and 4 μM thapsigargin (Tg) to promote global SR Ca^{2+} release and 50 μM *N*-benzyl-*p*-toluenesulfonamide (BTS) to prevent contraction. In both fibres, this produced a strong rise in fluo-3 fluorescence indicating that Ca^{2+} was well available in the SR compartment.

LY2940002 does not affect voltage-activated Ca^{2+} release

As results from Ca^{2+} transients in intact fibres suggested that accumulation of PtdIns(3,5)P_2 and/or PtdIns(3)*P* is capable of reducing voltage-activated Ca^{2+} release, it was of specific interest to explore the effect of manoeuvres intended to reduce the endogenous level of these compounds. For this, we first used LY294002, a classical pharmacological inhibitor of the different classes of PtdIns 3-kinases. Figure 4 compares indo-1 Ca^{2+} transients measured in a batch of control fibres and fibres injected with LY294002 so the final intracellular concentration was expected to be in the 0.1 mM range, well within the range expected to effectively block all classes of PtdIns 3-kinases (e.g., [21]). Fibres were subjected to the same voltage-clamp stimulation protocol as in Fig. 1 (Fig. 4a). Figure 4b shows the mean (±SEM) indo-1 saturation trace from the control (DMSO-injected) and from the LY294002-injected fibres and Fig. 4c shows the corresponding voltage dependence of peak Ca^{2+} release. Presence of the inhibitor clearly had no effect on Ca^{2+} release.

Overexpression of MTM1 does not affect voltage-activated Ca^{2+} release

PtdIns(3,5)P_2 and PtdIns(3)*P* are the main substrates of the PtdIns*P* phosphatase MTM1. An alternative possibility for reducing the level of these two PtdIns*Ps* was thus to overexpress MTM1; this was also of particularly strong interest since loss of activity of this phosphatase is responsible for severe pathological E–C coupling defects [1]. Figure 5 shows the expression pattern of a mCherry-tagged version of MTM1 expressed in a *fdb* muscle fibre, following in vivo transfection (see Material and Methods). Figure 5a–c illustrates the facts that mCherry-MTM1 was distributed throughout the entire volume of the fibres and, interestingly, that the fluorescence yielded a clear transversally striated component forming double rows spaced by ~2 μm, reminiscent of the triadic region. This was confirmed by co-localization of the mCherry fluorescence with that of t-tubule stained with di-8 anepps (Fig. 5d–f). Figure 6 shows the effect of exogenous MTM1

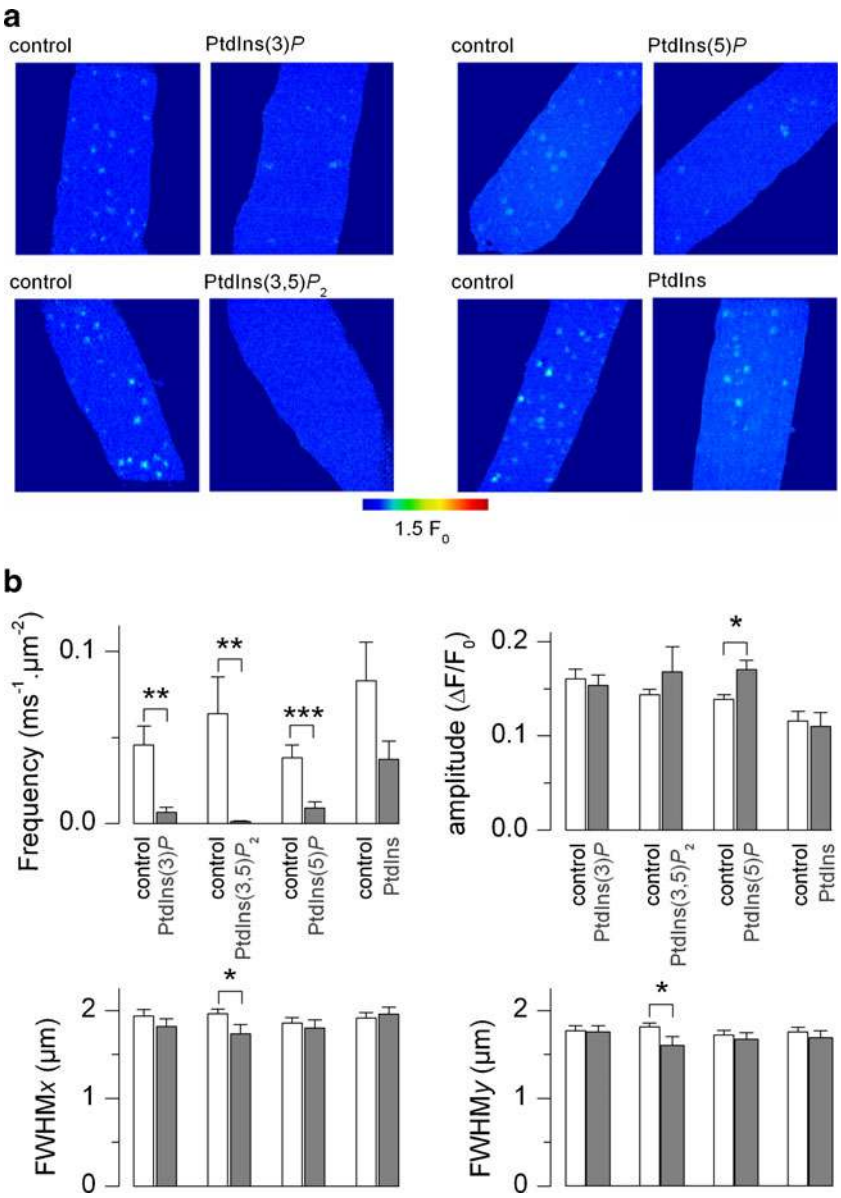

Fig. 3 Effect of PtdIns*P*s on spontaneous elementary Ca^{2+} release events in permeabilised muscle fibres. **a** Cumulated ECRE activity recorded with fluo-3 over a series of 200 consecutive confocal frames in fibres equilibrated with the indicated PtdIns*P* and in control fibres. **b** Mean values for the measured ECRE parameters in the different group of fibres. The number of fibres in the presence of a given PtdIns*P* and in the corresponding control group was 27 and 28 (PtdIns(3,5)P_2), 29 and 28 (PtdIns(3)*P*), 36 and 40 (PtdIns(5)*P*), 12 and 11 (PtdIns), respectively. All images are 84×84 µm

expression on voltage-activated Ca^{2+} release measured with indo-1. Figure 6b shows mean (±SEM) indo-1 saturation traces obtained from 11 control fibres and 11 mCherry-MTM1 expressing fibres in response to the pulse protocol shown in Fig. 6a; the corresponding voltage dependency of peak Ca^{2+} release is shown in Fig. 6c. Although there was a tendency for a slight reduction in peak Ca^{2+} release in the fibres overexpressing MTM1 as compared to control fibres, the difference was not statistically significant. Fitting a Boltzmann function to the data in each fibre gave mean values for maximum peak Ca^{2+} release, voltage of half-activation and steepness factor of 32.5±3 µM ms^{-1}, −7.2±1 mV, 6.8±0.2 mV and 28.2 ±3 µM ms^{-1}, −5.6±1 mV, 6.5±0.4 mV in control and MTM1-overexpressing fibres, respectively.

Indo-1 is a high-affinity dye that gets heavily saturated for large levels of step depolarization, a situation that could be thought to hamper detection of a putative enhancing effect of MTM1 overexpression on Ca^{2+} release; in order to make sure, Ca^{2+} transients from transfected fibres were also measured with fluo-4 in the presence of a high concentration of EGTA (see Materials and methods). In agreement with the indo-1 data, we — also in these conditions — found no indication that overexpression of MTM1 affected voltage-activated Ca^{2+} release: corresponding results are presented in Fig. S5 which shows the mean (±SEM) fluo-4 transients evoked by a 0.5-s-long depolarization from −80 to +30 mV in control fibres (n=5) and in fibres expressing mCherry-MTM1 (n=7), while Fig. S5c shows the corresponding Ca^{2+} release traces.

The possibility that the mCherry tag could somehow affect the activity of MTM1 so as to preclude a functional outcome was tested by measuring Ca^{2+} transients in fibres co-transfected with a plasmid encoding tag-free MTM1 and a plasmid

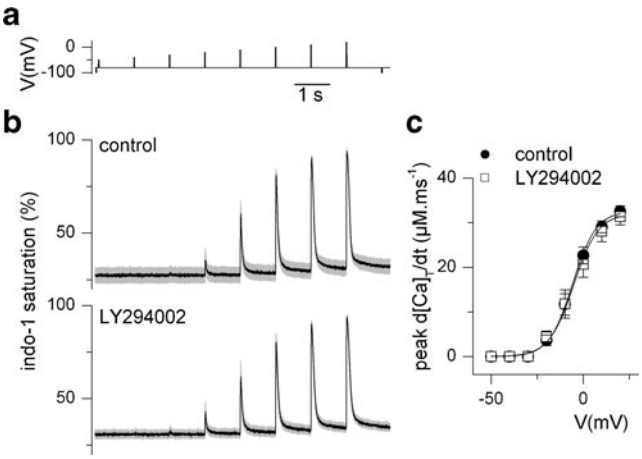

Fig. 4 Voltage-dependent Ca^{2+} release in fibres injected with the PtdIns-3 kinase inhibitor LY294002. **a** Voltage-clamp pulse protocol. **b** Mean (±SEM, *grey shading*) indo-1 saturation signal measured in fibres injected with LY294002 (n=6) and in the corresponding batch of control fibres (n=6). **c** Voltage dependence of mean peak values of Ca^{2+} release in the two groups of fibres. The trace superimposed to each set of data points corresponds to a Boltzmann function calculated with the mean parameters obtained from an individual fit of the function to the data points in each fibre. Mean values for maximum peak Ca^{2+} release, voltage of half-activation and steepness factor were 32.6±1 µM ms^{-1}, −5.8±2 mV, 6.4±0.3 mV and 32.1±2 µM ms^{-1}, −5.3±3 mV, 6.7±0.2 mV in control and LY294002-injected fibres, respectively

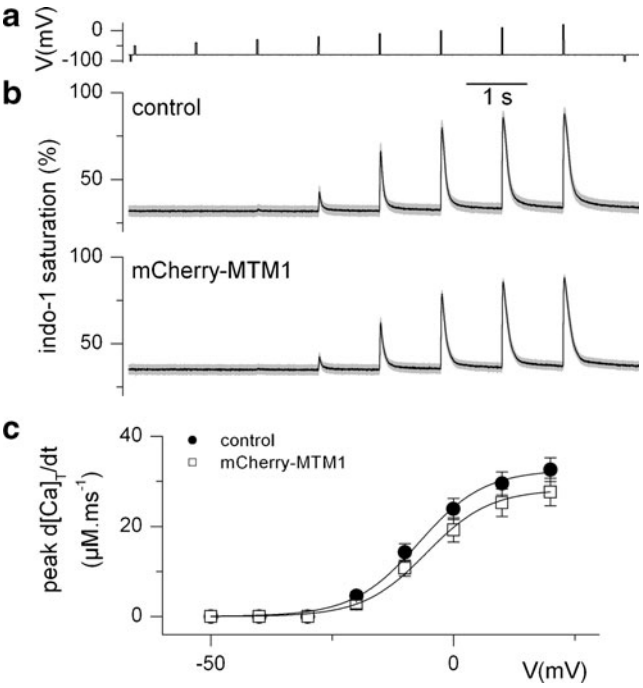

Fig. 6 Voltage-dependent Ca^{2+} release in fibres expressing mCherry-tagged MTM1. **a** Pulse protocol. **b** Mean (±SEM, *grey shading*) indo-1 saturation trace from control fibres (n=11) and from mCherry-MTM1 positive fibres (n=11). **c** Corresponding mean voltage dependence of peak Ca^{2+} release in the two sets of fibres

encoding EGFP. Voltage-activated Ca^{2+} transients in these fibres were compared to those measured in fibres transfected only with the EGFP plasmid. Results from these measurements are detailed in the Electronic supplementary material. They gave no indication that tag-free MTM1 would be more efficient than mCherry MTM1 in altering Ca^{2+} release. Finally, in another series of experiments, we also tested the possibility that the presence of exogenous MTM1 could affect Ca^{2+} release under more stringent conditions of muscle function. For this, Ca^{2+} transients were measured in fibres challenged by repeated trains of membrane depolarization; as described in Fig. S6 and in the corresponding text in the Electronic supplementary material, results also gave no insight into a possible effect of MTM1 overexpression on Ca^{2+} release.

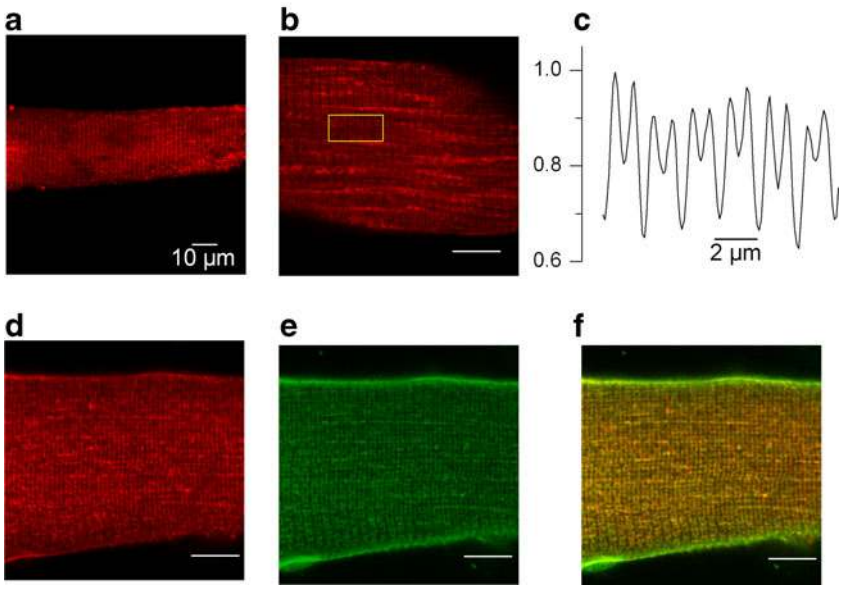

Fig. 5 Expression of the PtdIns*P*s phosphatase MTM1 in mouse muscle fibres. **a**–**b** Representative confocal images of the mCherry fluorescence from fibres expressing mCherry-tagged MTM1. **c** mCherry fluorescence profile along the x axis of the yellow box in **b**. **d**–**f** Co-localization of mCherry and di-8-anneps (*green*) fluorescence. Scale bars in the images all correspond to 10 µm

Concentration levels of PtdIns*P*s in muscle fibres

In order to estimate the physiological concentration levels of PtdIns*P*s in muscle fibres we used a high-performance liquid chromatography–mass spectrometry technique [7]. Although the technique cannot differentiate between the several mono- di- and tri-phosphorylated forms of PtdIns*P*, results were nevertheless anticipated to be informative in regard to the 100 μM concentration level of the several PtdIns*P*s forms we used in our injection experiments. The amount of PtdIns*P*, PtdInsP_2 and PtdInsP_3 present in fibres isolated from five *fdb* muscles is reported in Table 1; the estimated number of fibres in each sample is indicated in the right-end column. From these numbers, the mean concentration level of PtdIns*P* and of PtdInsP_2 was found to be 411±55 and 181±50 μM, respectively (n=5).

Discussion

The present work provides insights into a so-far-unexplored aspect of the E–C coupling function that has direct relevance to a fatal muscle disease. Indeed, the recent discovery that myotubular myopathy is associated with a severe alteration of Ca^{2+} release has highlighted the potentially critical role of PtdIns*P*s metabolism in the maintenance and/or regulation of this process. However, details of how PtdIns*P*s are involved in E–C coupling remain very mysterious.

We show that intracellular application of either PtdIns(3,5)P_2 or PtdIns(3)*P* depresses global voltage-activated Ca^{2+} release in intact muscle fibres. Conversely, we also show that two experimental strategies intended to reduce the level of these two 3-OH phosphorylated PtdIns have no effect on Ca^{2+} release, suggesting that they are maintained at an ineffective low-level in regard to this effect, in normal conditions.

Evidence for a role of PtdIns*P*s in the regulation of muscle Ca^{2+} homeostasis and/or E–C coupling is sparse: mainly, measurements of single RyR channel activity, Ca^{2+} release from SR vesicles and tension from skinned fibres suggested that PtdIns(4,5)P_2 has the potency to activate RyR1 [6, 20, 28] but no clear physiological correlate was ever provided. Our interest here was more specifically focused on the PtdIns*P*s species that are substrates or hydrolyzed products of MTM1. In relation to these, a set of relevant data was collected by Shen et al. [34] indicating that: (a) PtdIns(3,5)P_2 in cultured myotubes resides in the SR; (b) defects in myotubes Ca^{2+} signalling occur upon perfusion with PtdIns(3,5)P_2, PtdIns(3,4)P_2 or PtdIns(3)*P*; (c) all PtdIns*P*s bind to RyR1 with PtdIns(5)*P* yielding the highest binding activity; (d) PtdIns(3,5)P_2, in the 10–100 μM range, directly increases the activity of RyR1 as inferred for instance from the increased number of single RyR1 channel open events in reconstituted lipid bilayers. Although of strong relevance to the present issue, these results provided little insight into whether or not — and if so, how — PtdIns*P*s actually affect RyR1 function and E–C coupling in the native functional environment of an adult muscle fibre.

Our data provide evidence that physiologically triggered RyR1 function is sensitive to certain PtdIns*P*s: indeed data from intact fibres suggest that intracellular levels of PtdIns(3,5)P_2 or PtdIns(3)*P* in the 100 μM range depress voltage-activated Ca^{2+} release. The question of whether this concentration level of soluble di-C8 forms of PtdIns*P*s tested here has physiological relevance may be raised although a completely straightforward answer is harder to come by. From our measurements, we estimated the bulk concentration levels of PtdIns*P* and PtdInsP_2 in muscle fibres to be ~410 and 180 μM, respectively. In mammalian cells, the relative proportion of the three mono-phosphorylated forms of PtdIns*P* is considered to be 0.04 PtdIns(3)*P*, 0.04 PtdIns(5)*P* and 0.93 PtdIns(4)*P* (see [24]) which, according to the above value would correspond to ~16 μM PtdIns(3)*P* and PtdIns(5)*P* and ~380 μM PtdIns(4)*P*. For a muscle fibre assumed to be a cylinder of 25 μm diameter, considering the lipid membrane thickness to be 7 nm, the t-tubule to surface membrane ratio to be 6, the SR volume to represent 5.5% of total fibre volume [15] and the average inner SR radius to be 10 nm, one can calculate that the volume of surface membrane plus t-system membrane represents ~0.3% of the total fibre volume while the SR membrane volume represents ~4% of the total fibre volume. Thus, if distributed uniformly within the surface plus t-system plus SR membrane, the concentration of endogenous PtdIns(3)*P* and PtdIns(5)*P* should amount to 23 times their concentration in the fibre bulk, that is ~370 μM. The 100 μM concentration of PtdIns(3)*P* and PtdIns(5)*P* we used in our injection experiments corresponds to ~6 times the bulk endogenous levels. If the injected PtdIns(3)*P* and PtdIns(5)*P* also partition uniformly within the surface plus t-system plus SR membrane they would also reach a membrane concentration ~6 times larger than the endogenous levels. If they do not partition at all, the added 100 μM bulk level would then increase the concentration by a factor of ~1.3. The actual situation probably lies within these two limits.

Table 1 Quantification of PtdIns*P*s in muscle fibres

Sample	PtdIns*P* (ng)	PtdInsP_2 (ng)	PtdInsP_3 (ng)	Number of fibres
A	123.28	32.94	24.04	1026
B	99.86	32.05	10.94	1767
C	130.26	109.61	9.42	1463
D	96.17	43.88	6.4	1482
E	102.39	33.61	32.77	1273

Amount of mono-, di- and tri-phosphorylated PtdIns*P* measured in samples of muscle fibres isolated from five *fdb* muscles, as described in Materials and methods. The number of fibres estimated in each sample is indicated in the right-end column

Along the same line, the relative proportion of diphosphorylated forms of PtdIns*P* in mammalian cells is considered to be 0.002 PtdIns(3,4)P_2, 0.002 PtdIns(3,5)P_2 and >0.99 PtdIns(4,5)P_2 (see [24]), which according to our estimation of total PtdInsP_2 concentration would give 0.4 μM PtdIns(3,5)P_2. The 100 μM concentration of PtdIns(3.5)P_2 we used in our experiments thus corresponds to ~250 times this bulk level. If endogenous PtdInsP_2 distribute uniformly within the surface plus t-system plus SR membrane, the concentration of PtdIns(3,5)P_2 would amount ~9 μM. If the injected PtdIns(3,5)P_2 also partition entirely in these membranes its membrane concentration will also be 250 times larger than the endogenous level. Conversely, if it does not partition at all, the added 100 μM bulk level will then increase the concentration 11 times. Again, the actual situation has to stand within these two limits.

To summarize, the above estimations suggest that the injected 100 μM concentration of PtdIns*P*s increases the endogenous level of PtdIns(3)*P* and PtdIns(5)*P* by a factor of 1.3–10 and the level of PtdIns(3,5)P_2 by a factor of 11–250.

Increased levels of PtdIns(5)*P* and PtdIns(3,5)P_2 by a factor of 2–30 (which would more or less fit within the above ranges) have been reported in cell systems other than muscle, under various conditions of stress (see [24]). In the A431 epidermoid carcinoma model cell line, siRNA-mediated down-regulation of MTM1 expression resulted in a 1.4–2.5 increase in PtdIns(3)*P* level [4]. Consistently, Mtm1-null skeletal muscle was very recently reported to yield a 2.2-fold increase in PtdIns(3)*P* level as compared to wild-type muscle [2]. Overall, within the limits of the present knowledge, these numbers indicate that the 100 μM concentration of PtdIns*P*s we used may not be so far from the range of levels relevant to physiological or pathological conditions, although it may somewhat exceed such levels in the case of PtdIns(3,5)P_2.

We also examined the effect of PtdIns*P*s on Ca^{2+} release detected under the form of spontaneous elementary events. Normally, ECREs in mammalian muscle do not occur at a frequency that allows appropriate analysis, under physiological conditions. On the other hand, conditions that substantially increase their frequency, such as discussed here after saponin permeabilization, allow a connection between data measured in vitro (whether from vesicles or from artificial bilayers) and global calcium transients measured in intact muscle fibres. In other words, analysis of ECREs offers a way to address discrepancies of RyR1 function between a full in vitro situation and — as full as possible — physiological situation. Also considering that the physiological ECREs that build up the global Ca^{2+} transients in mammalian muscle fibres still remain poorly identified, this approach represents the best one can use to address elementary properties of RyR1-mediated Ca^{2+} release in situ. In qualitative agreement with the reduction of peak voltage-activated Ca^{2+} release by PtdIns(3,5)P_2 and PtdIns(3)*P* that we observed in intact fibres, we also found that the frequency of spontaneous Ca^{2+} release events was reduced by these two PtdIns*P*s in permeabilized fibres, although in contrast with data from intact fibres PtdIns(5)*P* also was effective under these conditions. According to the ECRE parameters, PtdIns*P*s effect on RyR1-mediated Ca^{2+} release is likely to result from a reduced occurrence of RyR1 channel opening than from an alteration of the channel conductance or of the number of coherently operating channels involved in a Ca^{2+} release event.

Our data complement the results of Shen et al. [34] showing that di-C8-PtdIns*P*s, at similar concentrations as used here, enhance the activity of RyR1 in vitro. Although these results may not seem intuitively consistent with the present ones, they may not necessarily be contradictory. Notice along this line that even within our study there was no full consistence between the intact and permeabilized fibre data with respect to PtdIns(5)*P* which had no significant effect on voltage-activated Ca^{2+} release while depressing the ECRE frequency. On the other hand, PtdIns(3,5)P_2 was found to be more effective in altering elementary release events than either PtdIns(3)*P* or PtdIns(5)*P*, in line with the observations made by Shen et al. [34]. Discrepancies may also reflect the different levels of complexity of PtdIns*P*s modulation of the RyR1 channel activity when going from the native intact muscle fibre environment with RyR1 under the control of the DHPR as compared to RyR1 spontaneous activity detected in permeabilized fibres under the form of ECREs and again versus the in vitro situation in vesicles or bilayer. One may for instance picture the possibility that a target other than RyR1 is involved in the effects at the single fibre level. In this respect, our data tend to exclude the DHPR, as evidenced from analysis of the membrane current measurements. Furthermore, the fact that ECRE, presumed to reflect a DHPR-free activity of RyR1 channels, also yield a depressed activity in the presence of PtdIns*P*s does not favour a role for the DHPR as a critical target. The enhanced PtdIns*P*s-induced RyR1 activity observed in vitro [34] could also be speculated to correspond to a specific effect on the resting level of RyR1 activity in the intact fibres; along such line, it is interesting that despite the reduced amplitude of voltage-activated Ca^{2+} release in fibres injected with PtdIns(3,5)P_2 and PtdIns(3)*P*, the resting [Ca^{2+}] level tended to be elevated.

One could have anticipated that under normal conditions, the endogenous level of PtdIns(3,5)P_2 and PtdIns(3)*P* has a chronic effect on Ca^{2+} release that could be overcome by further reducing the level of these molecules. This does not seem to be the case: despite yielding a pattern of expression consistent with the triadic region, overexpression of MTM1 left Ca^{2+} release unchanged. Along the same line, application of a PtdIns 3-kinase inhibitor which would have also been expected to reduce the endogenous level of PtdIns(3,5)P_2 and PtdIns(3)*P* was without effect. Together, these results provide no clue for the existence of a tonic effect of the endogenous

PtdIns*P*s on Ca^{2+} release in normal conditions. Interestingly along this line, recent results showed that ectopic expression in muscle of wild-type MTM1 did not induce any detectable signs of muscle alteration with respect to muscle weight, fibre size and isometric force, in agreement with the present results showing that the steps of E–C coupling remained essentially unaffected [2].

Altogether, although full understanding of the details of how PtdIns*P*s affect Ca^{2+} release in situ will necessitate more efforts, our results represent an important first step towards this goal. Also of importance, data highlight the possibility that accumulation of MTM1 substrates has the potency to depress Ca^{2+} release and to thus contribute to the defective E–C coupling in MTM1-deficient conditions [1]. The mechanism(s) involved and the actual PtdIns*P*s target(s) still remain speculative, and at present we cannot completely rule out that PtdIns*Ps* would act in a cell compartment other than the triadic region. Still, as shown for PtdIns(4,5)P_2 in regard to plasma membrane ion channels, PtdIns(3,5)P_2 and PtdIns(3)*P* may be suggested to exert their effect through a direct interaction with RyR1, and this is supported by the fact that several PtdIns*P*s do bind to RyR1 [34]. Alternatively, they could also be speculated to favor targeting or translocation of another protein in the vicinity of RyR1 or to induce structural changes in the triadic junction by altering membrane curvature [2] that would then be responsible for the observed effects.

Acknowledgements This work was supported by grants from Centre National de la Recherche Scientifique (CNRS), Université Lyon 1, Association Française contre les Myopathies (AFM), Hubert Curien Partnership Balaton (TeT_10-1-2011-0723) and OTKA K107765. E.G.R. was a recipient of a fellowship from the Spanish Ministry of Education and Science (MEC, José Castillejo Program). We thank Bruno Allard for critical comments on the manuscript and helpful discussion.

Ethical standards All experiments comply with the current laws of the two countries (France and Hungary) in which they were performed.

Conflict of interest The authors declare that they have no conflict of interest.

References

1. Al-Qusairi L, Weiss N, Toussaint A, Berbey C, Messaddeq N, Kretz C, Sanoudou D, Beggs AH, Allard B, Mandel JL, Laporte J, Jacquemond V, Buj-Bello A (2009) T-tubule disorganization and defective excitation-contraction coupling in muscle fibres lacking myotubularin lipid phosphatase. Proc Natl Acad Sci U S A 106: 18763–18768
2. Amoasii L, Hnia K, Chicanne G, Brech A, Cowling BS, Müller MM, Schwab Y, Koebel P, Ferry A, Payrastre B, Laporte J (2013) Myotubularin and PtdIns3P remodel the sarcoplasmic reticulum in muscle in vivo. J Cell Sci 126:1806–1819
3. Bolis A, Zordan P, Coviello S, Bolino A (2007) Myotubularin-related (MTMR) phospholipid phosphatase proteins in the peripheral nervous system. Mol Neurobiol 35:308–316
4. Cao C, Backer JM, Laporte J, Bedrick EJ, Wandinger-Ness A (2008) Sequential actions of myotubularin lipid phosphatases regulate endosomal PI(3)P and growth factor receptor trafficking. Mol Biol Cell 19:3334–3346
5. Cheng H, Lederer WJ, Cannell MB (2003) Calcium sparks: elementary events underlying excitation–contraction coupling in heart muscle. Science 262:740–744
6. Chu A, Stefani E (1991) Phosphatidylinositol 4,5-bisphosphate-induced Ca^{2+} release from skeletal muscle sarcoplasmic reticulum terminal cisternal membranes. Ca^{2+} flux and single channel studies. J Biol Chem 266:7699–7705
7. Clark J, Anderson KE, Juvin V, Smith TS, Karpe F, Wakelam MJ, Stephens LR, Hawkins PT (2011) Quantification of PtdInsP3 molecular species in cells and tissues by mass spectrometry. Nat Methods 8:267–272
8. Collet C, Csernoch L, Jacquemond V (2003) Intramembrane charge movement and L-type calcium current in skeletal muscle fibres isolated from control and mdx mice. Biophys J 84:251–265
9. Collet C, Pouvreau S, Csernoch L, Allard B, Jacquemond V (2004) Calcium signaling in isolated skeletal muscle fibres investigated under "Silicone Voltage-Clamp" conditions. Cell Biochem Biophys 40:225–236
10. Csernoch L, Bernengo JC, Szentesi P, Jacquemond V (1998) Measurements of intracellular Mg^{2+} concentration in mouse skeletal muscle fibres with the fluorescent indicator mag-indo-1. Biophys J 75:957–967
11. Csernoch L, Pouvreau S, Ronjat M, Jacquemond V (2008) Voltage-activated elementary calcium release events in isolated mouse skeletal muscle fibres. J Membr Biol 226:43–55
12. Di Paolo G, De Camilli P (2006) Phosphoinositides in cell regulation and membrane dynamics. Nature 443:651–657
13. Dowling JJ, Low SE, Busta AS, Feldman EL (2010) Zebrafish MTMR14 is required for excitation–contraction coupling, developmental motor function and the regulation of autophagy. Hum Mol Genet 19:2668–2681
14. Dowling JJ, Vreede AP, Low SE, Gibbs EM, Kuwada JY, Bonnemann CG, Feldman EL (2009) Loss of myotubularin function results in T-tubule disorganization in zebrafish and human myotubular myopathy. PLoS Genet 5:e1000372. doi:10.1371/journal.pgen.1000372
15. Eisenberg BR (1983) Quantitative ultrastructure of mammalian skeletal muscle. In: Peachey LD, Adrian RH, Geiger SR (eds) Handbook of physiology sect 10: skeletal muscle, 3rd edn. Williams & Wilkins, Baltimore, MD, pp 73–112
16. Hannon JD, Lee NK, Yandong C, Blinks JR (1992) Inositol trisphosphate (InsP3) causes contraction in skeletal muscle only under artificial conditions: evidence that Ca^{2+} release can result from depolarization of T-tubules. J Muscle Res Cell Motil 13:447–456
17. Harkins AB, Kurebayashi N, Baylor SM (1993) Resting myoplasmic free calcium in frog skeletal muscle fibres estimated with fluo-3. Biophys J 65:865–881
18. Jacquemond V (1997) Indo-1 fluorescence signals elicited by membrane depolarization in enzymatically isolated mouse skeletal muscle fibres. Biophys J 73:920–928
19. Kirsch WG, Uttenweiler D, Fink RH (2001) Spark- and ember-like elementary Ca^{2+} release events in skinned fibres of adult mammalian skeletal muscle. J Physiol 537:379–389
20. Kobayashi M, Muroyama A, Ohizumi Y (1989) Phosphatidylinositol 4,5-bisphosphate enhances calcium release from sarcoplasmic reticulum of skeletal muscle. Biochem Biophys Res Commun 163:1487–1491
21. Kong D, Dan S, Yamazaki K, Yamori T (2010) Inhibition profiles of phosphatidylinositol 3-kinase inhibitors against PI3K superfamily and human cancer cell line panel JFCR39. Eur J Cancer 46:1111–1121

22. Lanner JT, Georgiou DK, Joshi AD, Hamilton SL (2010) Ryanodine receptors: structure, expression, molecular details, and function in calcium release. Cold Spring Harb Perspect Biol 2:a003996
23. Laporte J, Hu LJ, Kretz C, Mandel JL, Kioschis P, Coy JF, Klauck SM, Poustka A, Dahl N (1996) A gene mutated in X-linked myotubular myopathy defines a new putative tyrosine phosphatase family conserved in yeast. Nat Genet 13:175–182
24. Lemmon MA (2008) Membrane recognition by phospholipid-binding domains. Nat Rev Mol Cell Bio 9:99–111
25. Logothetis DE, Petrou VI, Adney SK, Mahajan R (2010) Channelopathies linked to plasma membrane phosphoinositides. Pflugers Arch 460:321–341
26. Lukács B, Sztretye M, Almássy J, Sárközi S, Dienes B, Mabrouk K, Simut C, Szabó L, Szentesi P, De Waard M, Ronjat M, Jóna I, Csernoch L (2008) Charged surface area of maurocalcine determines its interaction with the skeletal ryanodine receptor. Biophys J 95: 3497–3509
27. Monnier N, Ferreiro A, Marty I, Labarre-Vila A, Mezin P, Lunardi J (2003) A homozygous splicing mutation causing a depletion of skeletal muscle RYR1 is associated with multi-minicore disease congenital myopathy with ophthalmoplegia. Hum Mol Genet 12:1171–1178
28. Ogawa Y, Harafuji H (1989) Ca-release by phosphoinositides from sarcoplasmic reticulum of frog skeletal muscle. J Biochem 106:864–867
29. Ohizumi Y, Hirata Y, Suzuki A, Kobayashi M (1999) Two novel types of calcium release from skeletal sarcoplasmic reticulum by phosphatidylinositol 4,5-biphosphate. Can J Physiol Pharmacol 77: 276–285
30. Pierson CR, Tomczak K, Agrawal P, Moghadaszadeh B, Beggs AH (2005) X-linked myotubular and centronuclear myopathies. J Neuropathol Exp Neurol 64:555–564
31. Pouvreau S, Csernoch L, Allard B, Sabatier JM, De Waard M, Ronjat M, Jacquemond V (2006) Transient loss of voltage control of Ca^{2+} release in the presence of maurocalcine in skeletal muscle. Biophys J 91:2206–2215
32. Pouvreau S, Jacquemond V (2005) Nitric oxide synthase inhibition affects sarcoplasmic reticulum Ca^{2+} release in skeletal muscle fibres from mouse. J Physiol 567:815–728
33. Romero-Suarez S, Shen J, Brotto L, Hall T, Mo C, Valdivia HH, Andresen J, Wacker M, Nosek TM, Qu CK, Brotto M (2010) Muscle-specific inositide phosphatase (MIP/MTMR14) is reduced with age and its loss accelerates skeletal muscle aging process by altering calcium homeostasis. Aging 2:504–513
34. Shen J, Yu WM, Brotto M, Scherman JA, Guo C, Stoddard C, Nosek TM, Valdivia HH, Qu CK (2009) Deficiency of MIP/MTMR14 phosphatase induces a muscle disorder by disrupting Ca^{2+} homeostasis. Nat Cell Biol 11:769–776
35. Suh BC, Hille B (2008) PIP2 is a necessary cofactor for ion channel function: how and why? Annu Rev Biophys 37:175–195
36. Szabó LZ, Vincze J, Csernoch L, Szentesi P (2010) Improved spark and ember detection using stationary wavelet transforms. J Theor Biol 264:1279–1292
37. Zhou H, Jungbluth H, Sewry CA, Feng L, Bertini E, Bushby K, Straub V, Roper H, Rose MR, Brockington M, Kinali M, Manzur A, Robb S, Appleton R, Messina S, D'Amico A, Quinlivan R, Swash M, Müller CR, Brown S, Treves S, Muntoni F (2007) Molecular mechanisms and phenotypic variation in RYR1-related congenital myopathies. Brain 130:2024–2036
38. Zhou H, Lillis S, Loy RE, Ghassemi F, Rose MR, Norwood F, Mills K, Al-Sarraj S, Lane RJ, Feng L, Matthews E, Sewry CA, Abbs S, Buk S, Hanna M, Treves S, Dirksen RT, Meissner G, Muntoni F, Jungbluth H (2010) Multi-minicore disease and atypical periodic paralysis associated with novel mutations in the skeletal muscle ryanodine receptor (RYR1) gene. Neuromuscul Disord 20:166–173
39. Zhou H, Yamaguchi N, Xu L, Wang Y, Sewry C, Jungbluth H, Zorzato F, Bertini E, Muntoni F, Meissner G, Treves S (2006) Characterization of recessive RYR1 mutations in core myopathies. Hum Mol Genet 15:2791–2803